DOI: 10.61782/fa.2025.0039

FORUM ACUSTICUM
EURONOISE 2025

A STUDY OF URBAN AIR MOBILITY ROTOR NOISE AT MODERATE REYNOLDS NUMBERS WITH COLLECTIVE PITCH CONTROL.

Charles E. Tinney[1†] **John Valdez**[1] **Yingjun Zhao-Dubuc**[1]
[1] Applied Research Laboratories, The University of Texas at Austin, Austin, Texas, USA
https://www.arlut.utexas.edu/gdl

ABSTRACT

Measurements of hover performance and acoustics of a Mach-tip scaled notional rotor for urban air mobility is presented. The blade shape is a 35% geometrically scaled replica of an earlier generation Joby rotor blade first studied by Tinney and Valdez [1] and is evaluated for changes to blade tip Mach number (between 0.28 and 0.40), rotor collective pitch angle, as well as rotor solidity (number of blades). The findings demonstrate that, in general, sound levels decay with increasing collective pitch angle, while they increase with increasing blade count. A delay in the collective pitch angle, where decreasing noise transitions to increasing noise with increasing collective, is also observed. When using thrust coefficient as the performance metric for comparing different rotor operating conditions, the transition point from decreasing noise to increasing noise is delayed to higher collective pitch angles as blade count increases. This tends to occur for the same range of rotor figures of merit between 0.65 and 0.70; peak hover efficiency is found for a figure of merit of 0.75. The findings provide a first principals understanding of the tradespace between hover performance and acoustics using a UAM relevant blade shape at Reynolds numbers of practical importance.

Keywords: *eVTOL, UAM, AAM, Rotor Noise.*

**Corresponding author*: ✉ *charles.tinney@arlut.utexas.edu.*

1. BACKGROUND

A low noise rotor capable of efficient take-off, landing and hovering operations is a prerequisite to the successful integration of urban air mobility (UAM) vehicles into the transportation network. This is an ambitious undertaking as the features of the blade that enhance propulsive efficiency in either hover or forward flight are different from the ones that are needed for low noise operations. To develop a blade shape that can satisfy all of these targets requires a contemporaneous understanding (either measured or simulated) of both rotor performance and its sound field, and at scales that are large enough to overcome Reynolds number effects. The last of these is problematic for most indoor test facilities and has averted the refinement of some rotor noise prediction methods, especially lower-fidelity approaches that lean on experimental validation for confidence. A second issue is concerned with identifying a metric that can capture community annoyance. One of the most commonly adopted metrics for static rotor noise tests is overall sound pressure level (OASPL). Corrections for human perception effects using well established weighting functions are easily incorporated into the OASPL metric and can improve insight into the effect of rotor operating conditions on community annoyance. Though these traditional metrics may not be the best indicators of annoyance, and one might consider other metrics that are designed to be sensitive to impulsive and distorted features in the acoustic waveform [2].

In this study, we present measurements from a test campaign performed in 2022 at The University of Texas at Austin to characterize the hover performance and acoustics of a notional UAM (or eVTOL) rotor blade. A description of this database was first presented by Tinney and Valdez [1] and focused mostly on reporting experi-

mental uncertainties and characterizing facility enclosure effects. Unlike a number of the laboratory-scale rotor tests being reported in the open literature using fixed pitch drone scale rotors, the rotor geometry studied here is a Mach tip scale rotor with collective pitch control, and with chord and twist distributions that are representative of the ones found on nearly all UAM platforms. An analysis of the trade-space between hover performance and perceived noise using this notional UAM rotor blade is presented for different blade number combinations and collective pitch settings of the rotor. The results are part of a larger effort by this group to characterize the performance and acoustic trade space of these unique UAM rotors and are complementary to the experimental and numerical studies reported by Brentner et al. [3], Baskaran et al. [4], and Pascioni et al. [5].

2. HARDWARE AND SETUP

Hover performance and acoustic measurements of a 35% scale UAM rotor were acquired in the Gas Dynamics Laboratory (GDL) of the Applied Research Laboratories, The University of Texas at Austin (ARL-UT). The GDL is a fully enclosed and acoustically treated laboratory encompassing $\dot{V} = 30,100$ ft^3 of climate controlled open air space over 1,500 ft^2 of floor space with an average ceiling height of 21 ft. ARL-UT is located in Austin, Texas near sea-level conditions ($p_\infty = 14.7$ psia (103,325 Pa), $T_\infty = 529$ R (294 K), $\gamma = 1.4$, $\rho = 2.33 \times 10^{-3}$ slug/ft^3) with a sound speed of air being estimated at $a_\infty = 1128$ ft/s. The blade is fabricated from 6061 aluminum using CNC machining and is a geometrically scaled replica of the blade shape flown on an earlier generation Joby Aviation prototype vehicle in 2017 and described recently by Stoll and Bevirt [6]. The 35% scale blade has a diameter of $D = 39.96$ in. (0.665 m) and has non-uniform chord and twist distributions, as shown in Fig. 1a where $cmax = 3.2976$ in. while the blade twist at the root is $\beta_0 = 26.15$ deg. Changes to rotor solidity were evaluated by changing the blade count from $N_b = 2$ to 5, thereby resulting in changes to the blade area from $A_b = 110$ in^2 to 276 in^2, respectively. Additional details concerning the GDL at ARL:UT, as well as the rotor and test stand are provided by Tinney and Valdez [1].

During testing, a magnetic rotary encoder tracks and records the angular speed and phase to within 0.0879 deg over the full duration of testing while a triad of hi-torque servos control collective pitch angles over the range $0 \leq \alpha \leq 18$ in $\delta\alpha = 3$ deg. increments. Blade pitch angles are routinely measured using a 0.1 deg accurate inclinometer while rotor collectives are referenced to a blade pitch angle of zero at $r = 0.75R$. An image of the 5-bladed rotor during testing is shown in Fig. 2. A test matrix of available databases that have been generated for this rotor is provided in Table 1. Symbols identified by (●) pertain to databases encompassing hover performance measurements only, whereas (▶) identify measurements comprising both performance and acoustics. Only a subset of this database will be used in the current discussion. The peak Reynolds numbers ($\mathrm{Re}_c = u(r)c(r)/\nu$) for these three rotor speeds occur at $r/R = 0.82$ and are valued at $Re_c = [3.7, 4.3, 4.9] \times 10^5$ with blade tip Mach numbers $M_t = \Omega R/a_\infty$ valued at 0.28, and 0.32, and 0.37, respectively.

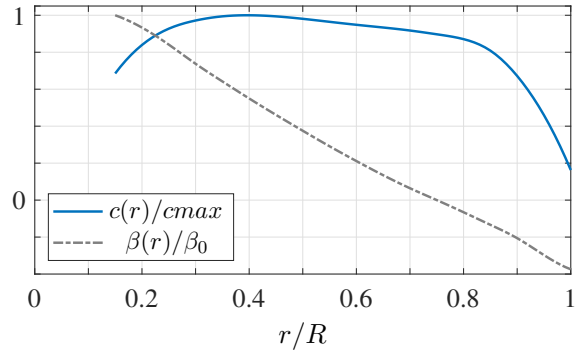

Figure 1. Chord and twist distribution of this notional UAM blade.

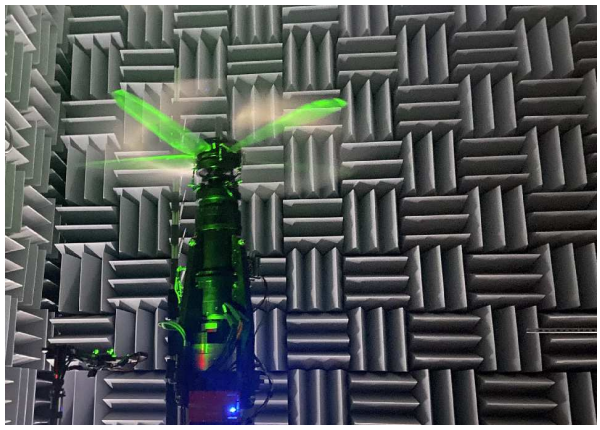

Figure 2. Testing of the notional UAM rotor with five blades.

N_b	σ	30 [rps]	35 [rps]	40 [rps]
2	0.088	▶	●	●
3	0.132	▶	▶	▶
4	0.176	▶	●	
5	0.220	▶	●	
	M_t:	0.28	0.32	0.37

Table 1. Test matrix of hover performance and acoustics of the 35% UAM rotor for all pitch angles ($\alpha = 0,\ 3,\ 6,\ 9,\ 12,\ 15$ deg).

3. HOVER SLIPSTREAM

Visualizations of the rotor slipstream were realized using a laser with sheet forming optics and a high-speed digital camera synchronized to the 1/rev magnetic encoded. The flow is seeded using a combination of atomized olive oil and glyceron fog with particle sizes ranging between 1-10μm; this is the same kind of setup used for Particle Image Velocimetry [7, 8]. The laser sheet is 2-3mm thick and is aligned with the quarter-chord of the blade to capture the tip-vortices, slipstream and blade wake generated by the different rotor configurations in hover. This is shown for the 3-bladed rotor in Fig. 3 at $\alpha = 12$ deg pitch and $M_t = 0.28$ (grid lines have increments of $0.1R$). The image is a pseudo-instantaneous snapshot made up of several images that are combine using Adobe Photoshop v.24. The process involves substitution (not addition or averaging) and works well for this kind of flow. Vortex centers are identified by hand (no vortex centering technique) and are labeled in degrees according to their wake age, ψ_v. The image is rich with information that is expected of this kind of flow. That is, the large radial displacement of the tip vortex up until the first blade pass is observed, followed by an abrupt change in its trajectory towards large axial displacements and increased vortex wander. Between the first and second blade passes, the blade wake passes from the roll-up of the first tip vortex, down to the second. The downwash reveals strong radial dependence at this rotor collective setting with the largest values residing at approximately 30% of the rotor radius. At higher rotor collectives (not shown) the downwash is relatively uniform across the slipstream. A broad range of turbulence scales are observed in the blade wake, while streamlines corresponding to the slipstream between subsequent blade wakes are smooth. This suggest that the rotor inflow is relatively free of turbulence.

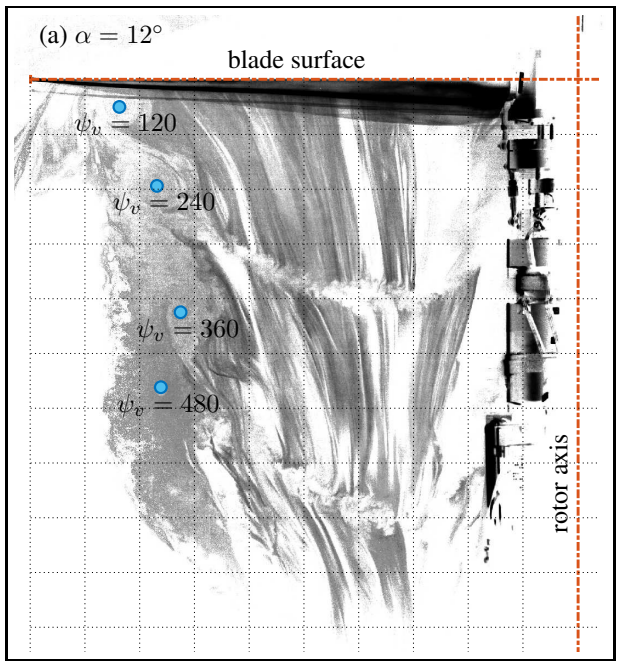

Figure 3. Visualization of the rotor wake generated by the 3-blade rotor at $\alpha = 12$ deg pitch and $M_t = 0.28$.

4. HOVER PERFORMANCE

Rotor torque and thrust were measured using an Interface Model 1216 bi-axial load cell with a 1000-lbf axial force T range (± 0.4 lbf) and a 500 lbf-in. torque Q range (± 0.35 lbf-in.). For each rotor condition, a minimum of three tests were conducted with each test encompassing 32.77 s of interrupted recordings. Measurements were recorded after the wake had stabilized and with the rotor disk elevated three rotor diameters above the facility floor [9]. Thrust coefficient $C_T = F_z/(\rho A(\Omega R)^2)$, power coefficient $C_P = \tau\Omega/(\rho A(\Omega R)^3)$ and rotor figure of merit $FM = C_T^{3/2}/(\sqrt{2}C_P)$ were calculated where $A = \pi D^2/4$ is the disk area, $\Omega = 2\pi\omega$ is the motor rotation speed in rad/s, and $P = Q\Omega$. Large changes in the facility time-scale ($t_v = \dot{V}/Av_i$ where $v_i = \lambda_i \Omega R$ is the rotor inflow and $\lambda_i = \sqrt{C_T/2}$), were observe and found to range from 351 s (for low collective settings of the 2-bladed rotor) to 96 s for the 5-bladed rotor at $\alpha = 15$ deg. collective. Blade loading coefficients (C_P/σ and C_T/σ) are shown in Fig. 4a for different blade number combinations and increasing collective pitch control. Hover efficiency is then reported in Fig. 4b for the same conditions

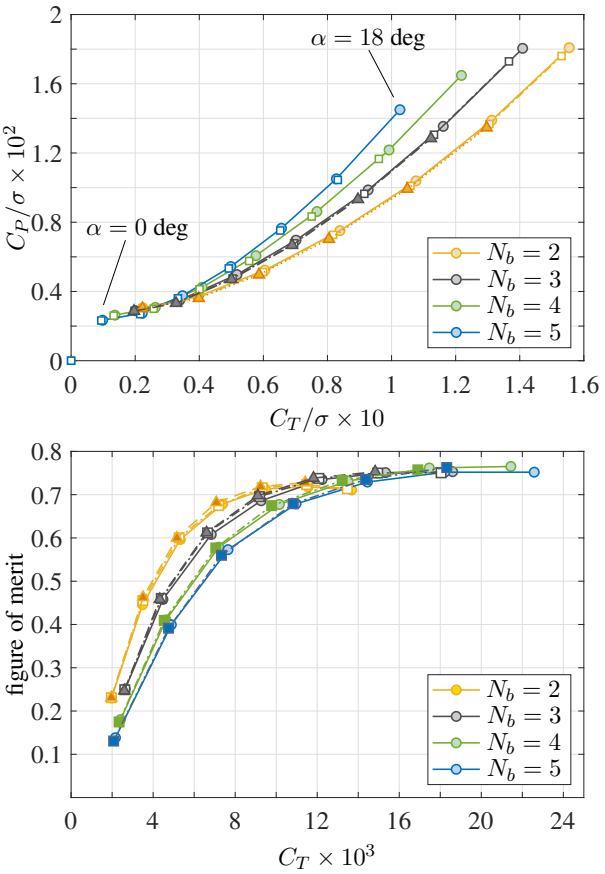

Figure 4. a) Blade loading coefficient and b) figure of merit for $M_t = 0.28$.

where colors are used to distinguish between blade numbers while symbols identify different rotor speeds. Low thrust coefficient and low figure of merit corresponds to low collective, while high thrust coefficient identifies the largest collective setting of the rotors. Peak figure of merit is valued at 0.75 and is achieved by the 4-bladed and 5-bladed rotors. The thrust coefficient where peak hover efficiency is achieved increases with blade count. For a given blade number count, increases to rotor speed have negligible effect on hover performance, thereby demonstrating that the performance of this scale rotor appears to be independent of Reynolds number effects.

5. HOVER ACOUSTICS

The sound field generated by this rotor was captured using a line array of 12 G.R.A.S. IEPE-type free-field microphones (combination of quarter-inch and half-inch capsules). Data was recorded uninterrupted for 20.48 s at 50 kHz sample rate using two NI-PXI-4472 boards (24-bit A/D converters with Butterworth filters). The microphone array was positioned so that the forth sensor was located at the rotor disk plane with remaining sensors being biased towards observers located below the rotor. The array was then traversed radially to create a 2D grid of measurements between $1.0 \leq r/D \leq 3.5$ in increments of $\delta r/D = 0.5$. Ensemble averaged sound pressure spectrum levels (SPSL, re: 20μPa) are computed using a hanning window with 75% overlap and a spectral resolution of $f_s/N = \delta f = 2.0345$ Hz. Microphone corrections (diffraction effects) are implemented following manufacturer guidelines [10]. In Fig. 5, a comparison between facility noise, motor noise and noise from the rotor are shown for an observer located below the rotor disk plane. Motor noise penetrates the rotor noise spectra at the fifth bpf harmonic, but is otherwise too low to contaminate the rotor noise measurement.

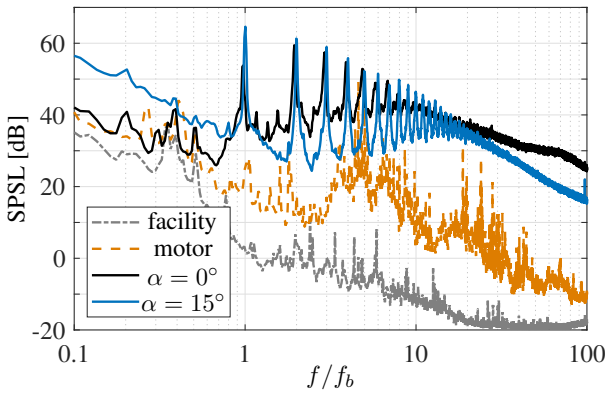

Figure 5. Sound pressure spectrum level [dB, re: 20μPa] of the facility background noise, motor noise and rotor noise at $M_t = 0.28$ for two pitch angles of the 5-bladed rotor as seen by a ground observer.

For the same observer and rotor operating conditions, the effect of blade pitch on the SPSL is shown in Fig. 6 with subsequent spectra being shifted by 20 dB to reduce clutter. An increase in rotor collective from $\alpha = 0$ deg to 6 deg is shown to shift rotor broadband noise to higher frequencies and is attributed to a reduction in blade vortex interaction noise. For $\alpha \geq 6$ deg, and higher, the characteristic frequency of the broadband noise hump is unaffected by changes in rotor collective, or the changes are too small to quantify.

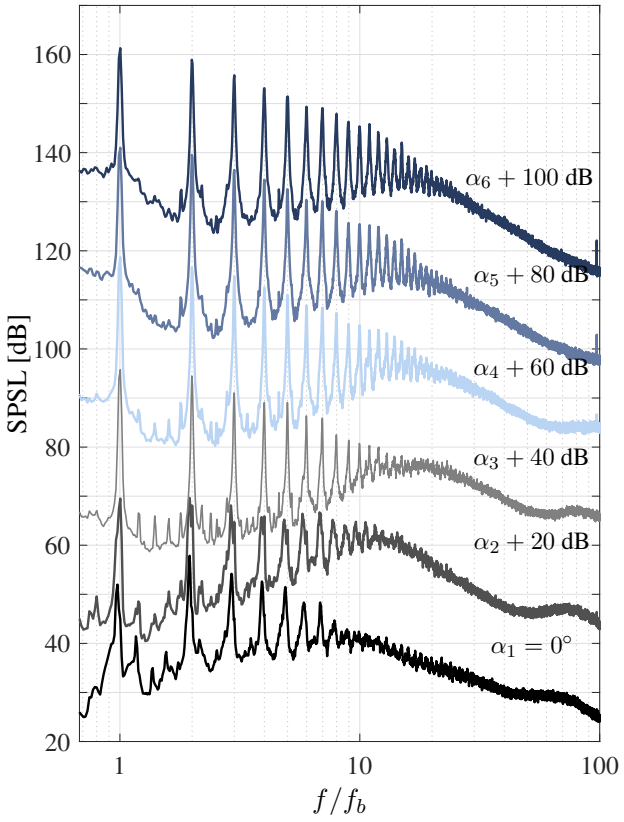

Figure 6. Effect of blade pitch angle on SPSL [dB] for an observer located at $r/D = 2.5$ at the a) rotor disk plane, and b) below ($\theta = -38$ deg). This is for the 5-bladed rotor at $M_t = 0.28$.

6. SCALING AND PERCEPTION

Rotor noise measurements are scaled to full scale conditions and then weighted using the A-weighting noise standard. Scaling is achieved by matching the product of Strouhol number with Mach number which produces Helmholtz number $H_m = fD/(\Omega R) \cdot M_{tip}$. Since blade tip Mach numbers are matched, the scaling reduces to changes in the source frequency using $f^* = \xi f$, where ξ is the geometrical scale factor between the laboratory and full-scale blades and is valued at 0.35. A demonstration of this is shown in Fig. 7 where both unweighted (dB) and weighted (dBA) SPSL are shown for an observer located below the rotor disk plane for the 5-bladed rotor at 30 rps and 15 deg blade pitch. As expected, the effect of A-weighting is a significant reduction in rotor harmonic noise, while rotor broadband noise remains unaffected and is now the dominant noise source. The high frequency peaks are electrical noise and are not related to the rotor or test stand.

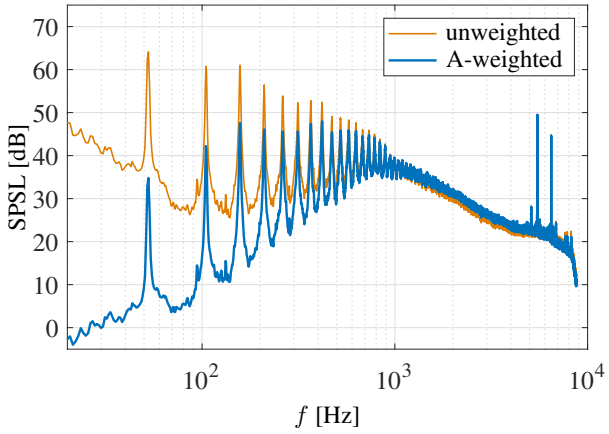

Figure 7. Scaled SPSL [dB] for the microphone observer located at $r/D = 3.05$ and $\theta = -35$ deg for the 5-bladed rotor operating at $M_t = 0.28$ and $\alpha = 15$ deg blade pitch.

The broader impacts of scaling and weighting the SPSL is demonstrated using contours of overall sound pressure level (OASPL) in Fig. 8 for the full 2D grid array. This is first demonstrated using the 3-bladed and 5-bladed configuration at $M_t = 0.28$ and $\alpha = 15$ deg pitch angle. Alongside these unweighted contours are contours of the scaled and weighted values. Comparing the two reveals the significant reductions in noise over all observer locations when human perception effects are included. As most of the low-frequencies associated with thickness and loading noise have been removed, self-noise from boundary layer turbulence on the pressure and suctions sides of the blade are shown to generate a sound field that is directive above and below the rotor. While these patterns signify dipole behavior, it is known that self-noise source mechanisms are quadrupoles and that their directivity is governed by the turbulence in the boundary layer whose spatial wavenumbers convect at speeds that allow them to become acoustically matched with the surrounding gas. The dipole shape is due to individual contributions of self-noise from the suction and high-pressure sides of the rotor. Fig. 8 shows this to be the case for both the 3-bladed and 5-bladed rotors.

Scaled and weighted SPSL are then evaluated in

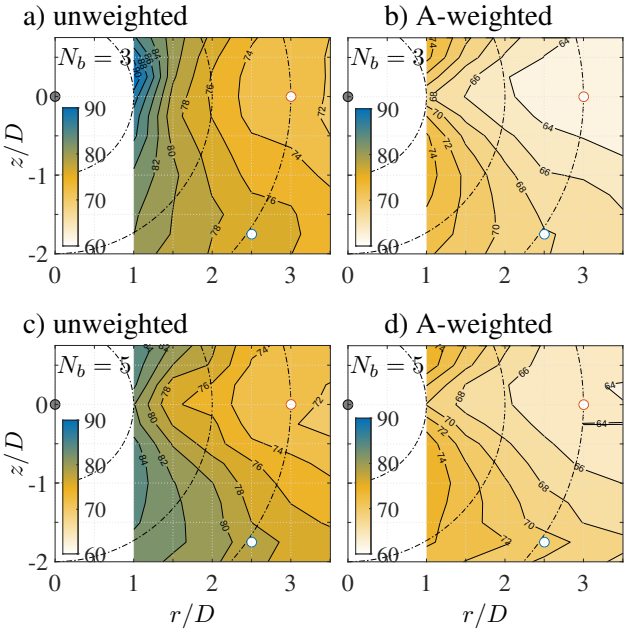

Figure 8. a,c) Unweighted and b,d) weighted OASPL at $M_t = 0.28$ and $\alpha = 15$ deg blade pitch for the a,b) 3-bladed and c,d) 5-bladed rotor.

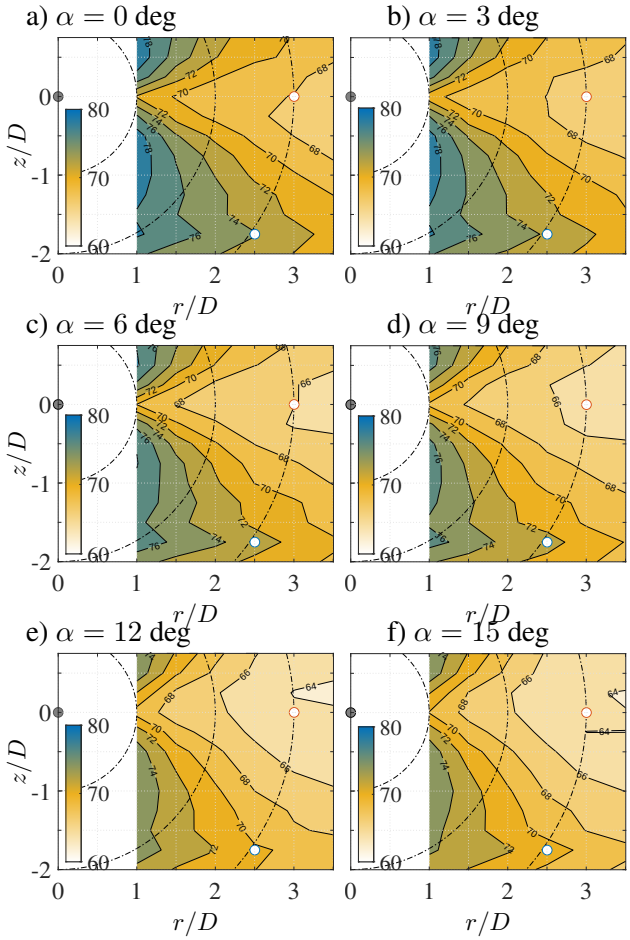

Figure 9. A-weighted OASPL at $M_t = 0.28$ for the 5-bladed rotor and all blade collective pitch angles.

Fig. 9 for all blade collectives to see the effect of rotor inflow on the self-noise. This is demonstrated using the 5-bladed rotor at $M_t = 0.28$. The contour decrements have been enhanced to accommodate the new A-weighted range of sound levels with each illustration comprising the same color scale so that direct comparisons can be made. The findings demonstrate negligible changes in contour shapes and sound directivity pattern on account of changes to rotor collective. Furthermore, OASPL levels are mostly unaffected by increasing rotor collective. In fact, at the highest collective pitch setting of $\alpha = 15$ deg, rotor noise amplitudes are shown to decrease over the entire observer space.

Scaled and weighted OASPL are now used to evaluate the trade-space between perceived noise and hover performance for all blade numbers and collective pitch settings. A presentation of findings from this can be overwhelming so the analysis is isolated to a single ground observer identified by blue circles in Figs 8 and 9; this is the same ground observer used to generate the SPSL in Fig. 7. The results are first reported in Figs. 10a and 10b without and with the effect of A-weighting, respectively, and with thrust coefficient as the performance metric. Starting with the 2-bladed and 3-bladed rotors, minimum perceived noise is achieved at moderate rotor collectives. As blade count advances to the 4-bladed and 5-bladed rotors, minimum perceived noise levels migrate towards higher rotor collectives thereby demonstrating that higher blade count rotors have increased inflow and subsequently generate more downwash which reduces the ingestion of turbulence from the wakes generated by preceding blades. For the 5-bladed configuration, the A-weighted noise decreases with increasing thrust, and complements the observations made concerning the contours in Fig. 9.

The same rotor conditions are then evaluated in Fig. 11 to reveal the trade-space between figure of merit and weighted/unweighted OASPL. For all blade number counts and at low hover efficiency conditions, as rotor collective increase, and consequently hover efficiency in-

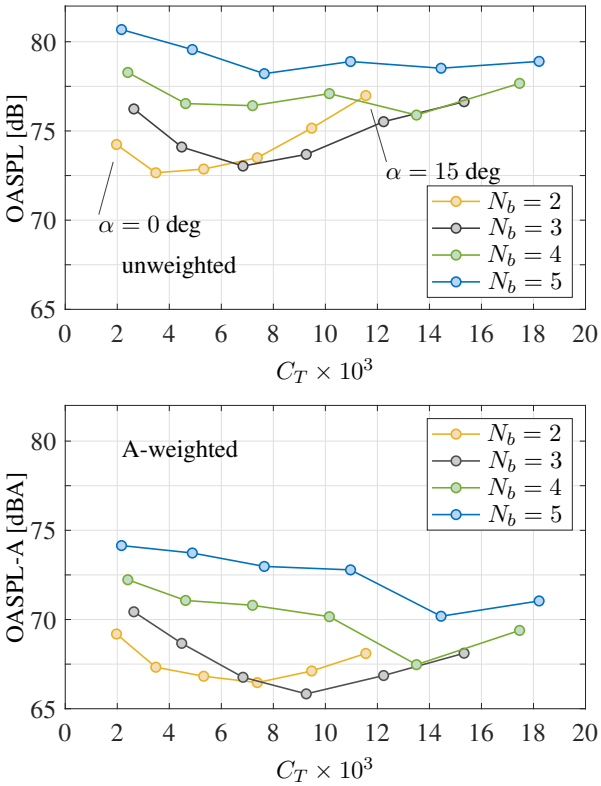

Figure 10. a) unweighted and b) weighted OASPL [dB] for the microphone observer located at $r/D = 3.05$ and $\theta = -35$ deg at $M_t = 0.28$.

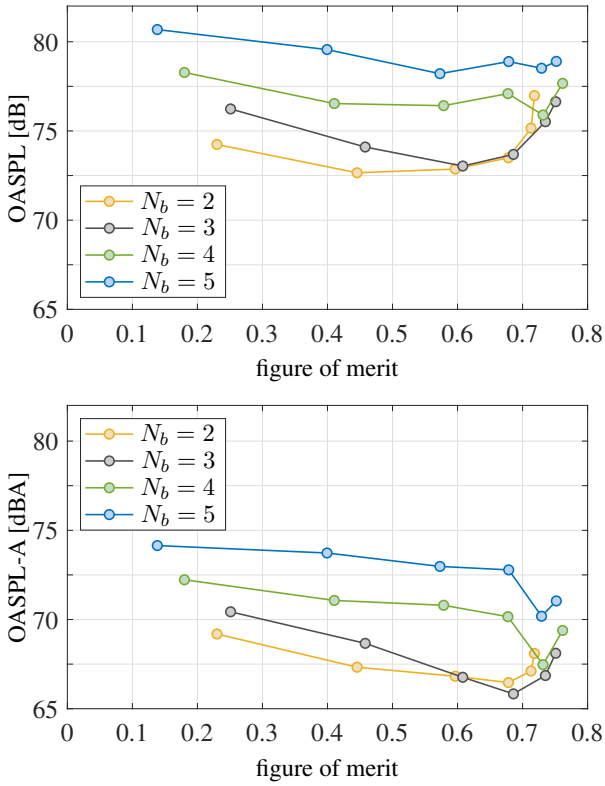

Figure 11. a) unweighted and b) weighted OASPL [dB] for the microphone observer located at $r/D = 3.05$ and $\theta = -35$ deg at 30 rps.

creases, perceived noise decreases. Eventually as the rate of change in hover efficiency begins to roll off, overall perceived noise levels begin to rise. This change is nearly consistent for all blade number combinations and occurs around a figure of merit between 0.65 and 0.7. The change is attributed to thickening of the boundary layers on the suction sides of the blades which promotes turbulence production. Regions of the blade close to the hub may be incipiently separated or stalled. Flow measurements / visualizations (like the one shown in Fig. 3) with the interrogation region being perpendicular to the rotor radius (complementary to the smoke visualizations of Yarusevych et al. [11]) are needed to address this question, and are currently underway. As hover efficiency approaches peak values of 0.75 for the different blade number counts, noise levels generated by all blade number combinations are within 3 dB for both the unweighted and A-weighted values.

7. SUMMARY

An analysis of hover performance and acoustics of a 35% scale UAM blade shape was presented using the experimental database described by Tinney and Valdez [1]. Performance measurements were acquired using a bi-axial load cell so that traditional metrics like thrust coefficient, power coefficient and rotor figure of merit were evaluated. The acoustic field was captured along a two-dimensional grid covering observer locations both above and below the rotor and between 1.0 and 3.5 rotor diameters from the hub; pressure measurements in this region are shown to transition from hydrodynamic to acoustic waveforms. Both hover performance and acoustics are evaluated for changes to the rotor collective pitch angle and for different blade number counts as well as increasing rotor speed (tip Mach numbers ranging between 0.28 and 0.37). At this scale, rotor performance was shown to be independent of Reynolds numbers while the thrust coefficient where peak

hover efficiency resided increased with increasing blade count. Contour maps of unweighted and A-weighted overall sound pressure levels were then evaluated for different collective pitch settings of the 3-bladed and 5-bladed rotor and by scaling the rotors to match full-scale conditions. As expected, a significant increase in loading noise and self-noise (rotor broadband noise) was observed while thickness noise, which is predominantly monopole-like, was suppressed. When the blade count advanced from a 4-bladed rotor to a 5-bladed rotor, minimum perceived noise levels were shown to migrate towards higher rotor collectives thereby demonstrating that higher blade count rotors have increased inflow and subsequently generate more downwash. The additional downwash reduces the ingestion of turbulence from the wakes generated by preceding blades.

8. ACKNOWLEDGMENTS

Support for this effort was graciously provided through an internal research and development award with the Signal and Information Sciences Laboratory of the Applied Research Laboratories, The University of Texas at Austin.

9. REFERENCES

[1] C. E. Tinney and J. Valdez, "Hover performance and acoustics of a 35% scale notional evtol rotor," *AIAA Paper 2024-3219*, pp. 1–14, 2024.

[2] C. E. Tinney and J. Valdez, "Higher-order statistical metrics for characterizing multirotor acoustics," *AIAA Journal*, vol. 62, no. 11, pp. 4431–4441, 2024.

[3] K. S. Brentner, B.-E. Zolbayar, and T. F. Jaworski, "An investigation of noise from electric, low-tip-speed aircraft propellers," *in: AHS International Technical Meeting on Aeromechanics Design for Transformative Vertical Flight*, pp. 1–10, 2018.

[4] K. Baskaran, N. S. Jamaluddin, A. Celik, and D. Rezgui, "Effects of number of blades on propeller noise," *Journal of Sound and Vibration*, vol. 572, no. 118176, pp. 1–17, 2024.

[5] K. A. Pascioni, A. C. Thai, and J. J. Bain, "Propeller source noise separation from flight test measurements of the joby aviation aircraft.," *AIAA Paper 2024-3231*, pp. 1–14, 2024.

[6] A. Stoll and J. B. Bevirt, "Development of evtol aircraft for urban air mobility at joby aviation," *Vertical Flight Society Forum 78, Paper 2022-17528*, 2022.

[7] S. Mula, J. Stephenson, C. E. Tinney, and J. Sirohi, "Dynamical characteristics of the tip vortex from a four-bladed rotor in hover," *Experiments in Fluid*, vol. 54, no. 1600, 2013.

[8] S. Mula and C. E. Tinney, "A study of the turbulence within a spiralling vortex filament using proper orthogonal decomposition," *Journal of Fluid Mechanics*, vol. 769, pp. 570–589, 2015.

[9] E. A. Fradenburgh, "The helicopter and the ground effect machine," *Journal of the American Helicopter Society*, vol. 5, pp. 24–33, 1960.

[10] S. Rayes, "How to match a measurement microphone to a sound field," *G.R.A.S. Sound and Vibration Handbook*, p. 12, 2021.

[11] S. Yarusevych, P. E. Sullivan, and J. G. Kawall, "On vortex shedding from an airfoil in low-reynolds-number flows," *Journal of Fluid Mechanics*, vol. 632, pp. 245–271, 2009.